



HAL
open science

Impacts of laser cooling for low earth orbit observation satellites: An analysis in terms of size, weight and power

Rémi Vicente, Gilles Nogues, Jean-Michel Niot, Thierry Wiertz, Pierre Contini, Arnaud Gardelein

► To cite this version:

Rémi Vicente, Gilles Nogues, Jean-Michel Niot, Thierry Wiertz, Pierre Contini, et al.. Impacts of laser cooling for low earth orbit observation satellites: An analysis in terms of size, weight and power. *Cryogenics*, 2020, 105, pp.103000. 10.1016/j.cryogenics.2019.103000 . hal-03488413

HAL Id: hal-03488413

<https://hal.science/hal-03488413>

Submitted on 7 Mar 2022

HAL is a multi-disciplinary open access archive for the deposit and dissemination of scientific research documents, whether they are published or not. The documents may come from teaching and research institutions in France or abroad, or from public or private research centers.

L'archive ouverte pluridisciplinaire **HAL**, est destinée au dépôt et à la diffusion de documents scientifiques de niveau recherche, publiés ou non, émanant des établissements d'enseignement et de recherche français ou étrangers, des laboratoires publics ou privés.



Distributed under a Creative Commons Attribution - NonCommercial 4.0 International License

Impacts of laser cooling for low earth orbit observation satellites: an analysis in terms of size, weight and power

Rémi Vicente^{a,b,*}, Gilles Nogues^b, Jean-Michel Niot^a, Thierry Wiertz^a, Pierre Contini^a and Arnaud Gardelein^{a,**}

^a*Air Liquide Advanced Technologies, 38360 Sassenage, France*

^b*Université Grenoble Alpes, CNRS, Institut Néel, 38000 Grenoble, France*

ARTICLE INFO

Keywords:

Laser cooling in solids
Solid state optical cryocooler
Vibration free cryocooler
Low earth orbit satellite
Infrared observation mission
Feasibility study
Satellite trade-off
Spacecraft integration
Size, weight and power analysis

ABSTRACT

Laser cooling in solids is a breakthrough technology allowing vibration-free cooling down to a temperature of 100 K in a miniaturized way. It appears as a promising technology to improve future observation satellites performances e.g. in SWIR and NIR domains.

In this paper, integration of a laser cooler onboard an observation satellite is studied for the first time. Our study focuses on size, weight and power (SWaP) criteria, at both satellite payload and platform levels. Its goal is to assess the interest of using an optical cryocooler over a mechanical cryocooler for low earth orbit (LEO) infrared observation missions.

A preliminary space-borne laser cooler (LC) architecture is proposed. It is composed of two parts. The first part is the cooling head, based on state-of-the-art cooling crystals 10%Yb:YLF and an astigmatic multipass cavity. The second part is the cryocooler opto-electronics, based on redundant laser diodes and fiber coupled to the cooling head. The cooling power is estimated for a small focal plane, taking into account the thermal load of an infrared detector and the parasitic heat fluxes inside the cryostat. The required optical and electrical powers of the laser cooler are then estimated considering the crystal efficiency, the thermal link losses and the opto-electronics efficiency.

Assuming a 5-year long LEO microsatellite mission, the sizing of the electrical power systems (PCDU, solar array, batteries) and thermal control systems (heatpipes, radiators) is performed. An additional mass margin is added to take mechanical support structures into account. At the end, payload and platform masses and volumes are summed respectively to obtain a SWaP balance at satellite level, representative of the overall impact of a laser cooler. The study is repeated for the case of a Miniature Pulse Tube Cooler (MPTC) architecture under the same mission and platform assumptions. Finally, the two architectures are compared. It is shown that even if the power requirement of a laser cooler is high, the reduction of mass and internal volume makes it possible for small satellite payloads.

1. Introduction

Laser cooling in solids is a breakthrough technology taking advantage of the interaction between an infrared laser and an ultra-pure rare-earth doped crystal in order to generate cold. Since its first demonstration in the 90s [1], the main research drive behind laser cooling has always been vibration-less cryocooling for space applications [2]. Indeed, it is the only all-solid-state active cooler able to reach temperatures lower than 180 K.

At the time, prospective studies have been made to quantify the performances of a laser cooler compared to other coolers in the same temperature range: pulse tube coolers and thermoelectric coolers [3, 4]. Much progress have been achieved since then, allowed by improved crystal growth quality [5], new optical cavities design [6] and optimized thermal links [7]. Laser cooling is an increasingly mature technology, each year improving in efficiency, and its minimum achievable temperature is expected to reach liquid nitrogen temperature [8]. Moreover, it is already capable of cooling an operating infrared Fourier transform spectrometer (FTIR) down to 135 K [9].

In this paper, the performances and impacts of a laser

cryocooler architecture for focal plane integration onboard an infrared observation satellite are reviewed. To the authors knowledge, no study has been made so far to assess the in-details impacts of a laser cooler at satellite level although this is a critical point to consider. Indeed, a laser cooling device is expected to be lightweight and compact due to the absence of mechanisms and the reduced size of cooling crystals employed (typical dimensions $10 \times 4 \times 4$ mm [10]). However, several tens of watts of laser power are needed to provide sufficient heat lift in order to cool a detector at cryogenic temperature, requiring adequate solar array, batteries and thermal control sizing.


Starting from a baseline low earth orbit (LEO) mission scenario, this study focuses on the size, weight and power aspects (SWaP) of a state-of-the-art laser cooler (LC), first at payload level and then at platform level. To make a comparison with an existing space cryocooling technology, the SWaP at satellite level for a Miniature Pulse Tube Cooler architecture (MPTC) is reviewed as well. Finally, the fundamental differences and predicted advantages of a laser cryocooler for LEO observation satellites are given.

2. Mission scenario

This study is based on a typical LEO satellite infrared observation mission such as Microcarb (CNES, 2021) [11].

*Corresponding author

**Principal investigator

 remi.vicente@airliquide.com (R. Vicente)

ORCID(s): 0000-0003-3785-3018 (R. Vicente)

Table 1
Satellite mission synthesis

Orbit	SSO
Altitude	650 km
Orbital period	98 min
Eclipse time	34 min
MLT (descending node)	10h30
Mean beta angle	22.5 °
Mission duration	5 years

The hypothesis of a high reliability 5 years mission is made, with continuous observation time (>95 % observation disponibility).

2.1. Orbit hypotheses

A quasi-circular sun synchronous orbit with 650 km altitude, 98 ° inclination and 10h30 mean local time of ascending node is assumed. The beta angle, defined as the angle between the satellite's orbital plane and the Earth-Sun vector is used to estimate the eclipse time. For a 10h30 orbit, the mean beta angle over 1 year is 22.5 ° [12]. The orbital period T is calculated using the formula [13]:

$$T = 2\pi \sqrt{\frac{(R_e + h)^3}{GM_e}} \quad (1)$$

with $R_e = 6371 \cdot 10^3$ m the Earth radius, h the altitude, $G = 6.674 \cdot 10^{-11}$ m³kg⁻¹s⁻² the gravitational constant and $M_e = 5.972 \cdot 10^{24}$ kg the Earth mass. Taking $h = 650 \cdot 10^3$ m, an orbital period of $T = 5855$ s = 98 min is found. The eclipse fraction f_E is calculated using the formula [13]:

$$f_E = \frac{1}{\pi} \cos^{-1} \left(\frac{\sqrt{h^2 + 2Rh}}{(R + h)\cos(\beta)} \right) \quad (2)$$

Replacing beta with its value, we find $f_E = 0.35$, leading to an eclipse time of $T_E = 0.35 \times 98 = 34$ min. Mission parameters are summarized in Table 1.

2.2. Focal plane thermal budget

A focal plane embedding an infrared HgCdTe detector, model Sofradir NGP SWIR (1024 × 1024 pixels, 15 × 15 μm pitch) is considered. This detector has a thermal dissipation of typically 150 mW [14]. Other heat sources inside the cryostat are:

- The conductive losses coming from the focal plane supporting blades.
- The conductive losses coming from the electrical connections.
- The radiative flux hitting the detector and the focal plane.

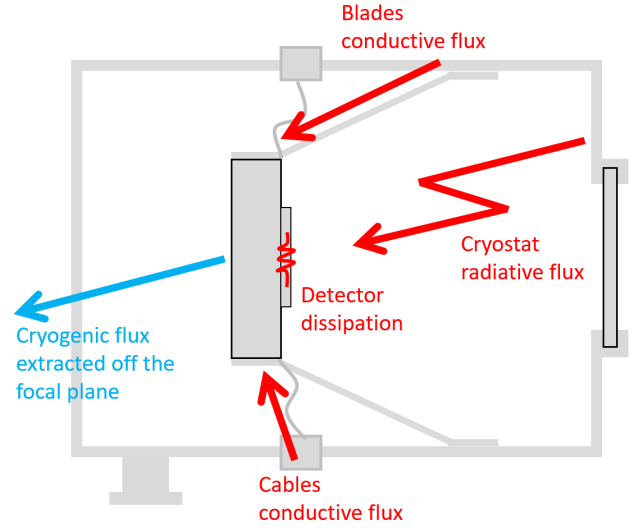


Figure 1: Schematized heat sources in the focal plane

Table 2
Estimated heat sources in the focal plane

Item	Heat flux (mW)
Detector	150
Focal plane supporting blades	65
Electrical connections	35
Radiative flux on detector	15
Radiative flux on focal plane	15
Total	280 mW

The heat sources in the focal plane are schematically presented in Figure 1. Their estimated heat load values are summarized in Table 2. A total heat load of 280 mW needs to be extracted off the focal plane in order to cool the detector.

In practice, the cooling power of a cryocooler has to be higher to compensate for thermal losses coming from its architecture (internal losses and cold redundancy). Thermal losses are taken into account in subsection 4.3.2 for the LC architecture and subsection 5.4.2 for the MPTC architecture.

2.3. Power distribution specifications

As a general rule, high satellite bus power requires a large power control and distribution unit (PCDU). For a micro-satellite, the assumption is made that moderns PCDUs such as the Myriade Evolution PCDU are highly efficient, modular and can withstand an extra 100 W payload equipment with marginal mass increase [15]. PCDU and satellite power regulation electronics masses are hence not considered in this study.

2.4. Solar array specifications

The solar array considered is a one-axis oriented array, able to keep the solar beta angle during the satellite revolution, assuring nearly constant solar irradiance during day time. The array is composed of triple junction Ga/As solar

Table 3

Solar array power, mass and size specifications

Solar power conversion efficiency	30 %
Surface power density BOL	410 W/m ²
Inherent array degradation	75 %
PCDU conversion efficiency	95 %
Corrected surface power density BOL	292 W/m ²
Degradation rate	4 %/year
Lifetime degradation	82 %
Surface power density EOL	240 W/m ²
Surface mass	2.5 kg/m ²
EOL power to mass ratio	96 W/kg
Thickness	25 mm

cells, with 30 % solar efficiency [16]. The beginning of life (BOL) surface power density of a solar array is given by:

$$\phi_{BOL} = \eta_{SA} F \quad (3)$$

With ϕ_{BOL} the surface power density in W/m², η_{SA} the array efficiency and $F = 1367 \text{ W/m}^2$ the solar constant. This yields a surface power density of:

$$\phi_{BOL} = 1367 \times 0.3 = 410 \text{ W/m}^2 \quad (4)$$

The BOL surface power density is then corrected to take into account: the inherent degradation of the solar cells due to panels heating and view factors between the satellite and the solar array, the conversion efficiency from the solar array to the PCDU. Assuming an inherent degradation of 75 % due to view factors and heating of the solar cells [13] and 95 % conversion efficiency from the solar array to the PCDU, a corrected surface power density of 292 W/m² is found. The lifetime degradation L is calculated using the formula:

$$L = (1 - \delta)^N \quad (5)$$

with δ the array's annual degradation due to irradiation in LEO and N the number of years in orbit. Taking an annual degradation $\delta = 4\%$ and a mission life of $N = 5$ years, the lifetime degradation is $\sim 82\%$. The end of life (EOL) power density amounts to 220 W/m². Surface mass of a solar array is estimated to 2.5 kg/m² [17], yielding an intrinsic EOL power per mass ratio of 96 W/kg. The panel thickness was estimated to 25 mm based on recent array technologies [18]. The solar array mass and power specifications are summarized in Table 3.

Finally, the mass augmentation of the solar array drive mechanisms and the inertia wheel due to the oversizing of the solar array is taken into account in the structure margin and supporting margin presented in subsection 2.7.

2.5. Batteries specifications

A battery composed of Saft VES16 Li-Ion cells [19] is considered. Indeed, this cell model is recent, space qualified and its small capacity makes it suitable for low power missions. Furthermore, its discharge performances have been assessed for LEO missions [20].

Table 4

Li-ion cells specifications

Model	Saft VES16
Type	Li-ion
Capacity	4.5 Ah
Voltage	3.6 V
Dimensions	60 mm × ø33 mm

Considering one charge/discharge cycle per satellite revolution, a 5 years mission duration with 98 minutes orbital period yields approximately 27000 cycles. From the batteries specifications, with 30 % depth of discharge (typical value for LEO missions), the battery capacity fading after 27000 cycles is estimated to 88 % [21].

2.6. Thermal control

The heat dissipated by a cooling system such as a laser cooler or a pulse tube cooler needs to be evacuated to avoid any system malfunction. Only thermal control for the cryocooling sub-systems is considered. The assumption is made that driving electronics are made in contact with the external satellite faces acting as a radiator which dissipates the heat into space. Hence it does not require additional thermal control.

Thermal control sizing depends on the cooler's thermal dissipation. LC and MPTC require the use of heat pipes with a diameter sized to the maximal extracted heat flux [22]. Each heat pipe is in contact with a radiator. On a satellite, a radiator facing outer space with an infrared emissivity $\epsilon = 0.85$ has a temperature of 280 K. It typically dissipates 300 W/m² [23]. In practice, this value is halved to account for equipment-radiator temperature gradients and illumination from the sun or the solar array, yielding an effective heat dissipation of 150 W/m². Assuming a 1.5 mm thick aluminum sheet with a density of 2700 kg/m³, the surface mass of a radiator panel is approximately 4 kg/m².

2.7. Structure and supporting margin

Structure and supporting of the equipments is estimated to 20 % of the total mass in a satellite [24]. To reach that value, a +25 % margin on the final satellite mass is applied. The margin is calculated as follows: Assuming M the final mass with margins, m the final mass without margin and x the structure and supporting mass, we have the relationship $M = m + x$ and $x = M \times 0.2$. This yields $x = (m + x) \times 0.2$. Rearranging, the mass margin is found as $x = m/(1 - 0.2) = m/0.8 = m \times 1.25$

3. Laser cooler preliminary architecture

There are two main designs of laser coolers, depending if the cooling crystal is located within the laser source's cavity (intra-cavity design) or separated from the laser part (extra-cavity design). An extra-cavity design is considered here.

An extra-cavity laser cooler is divided into two sub-systems. The first one is the optical cavity containing the cooling crys-

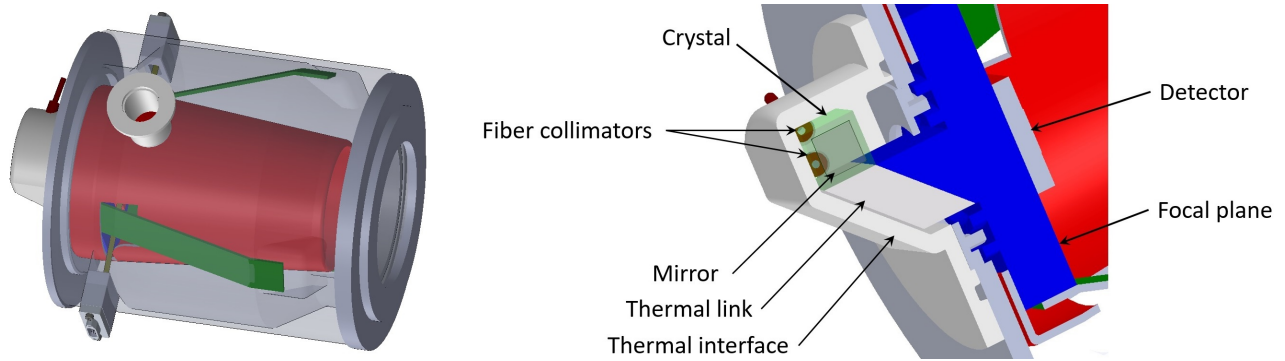


Figure 2: **Left:** Concept of a focal plane architecture with a laser cooler. The opto-electronics part (LEA) is not shown. The scale is the same as Figure 5. **Right:** Side cut of the cold head (CLOE).

tal, linked with a thermal link to the load. This part is responsible for the cooling process and needs to be supplied with optical power from a laser going through the cavity. It is referred as Cryogenic Laser Optical Exchanger (CLOE).

The second sub-system is the electronic module generating the optical power and feeding it to the cavity through an optical fiber. It contains the power conversion electronics, the laser diodes, and the control/command module needed to operate the system. It is referred as Laser Electronics Assembly (LEA). The general architecture of a laser cooler is shown in Figure 3. The features of these two sub-systems are detailed in the next sections.

3.1. Cryogenic Laser Optical Exchanger

The Cryogenic Laser Optical Exchanger (CLOE) sub-system role is to:

- Convert the input optical power into cooling power extracted off the thermal load.
- Report the cryogenic temperature to the LEA.

The cooling material, a rare-earth doped crystal is held at the center of a multipass optical cavity [6], whose purpose is to increase the interaction length between the laser beam and the material.

The cavity is made of two ultra-high reflection mirrors facing each-others. The walls of the cavity are coated with low thermal emissivity, high near-infrared absorption coating, such as TiNOX [25] or Nano Black [26]. The goal is to absorb a maximum of fluorescence radiation coming from the crystal while maintaining low thermal radiation load between the ambient temperature enclosure and the cold crystal.

A thermal link is attached between the crystal and the load to be cooled. The thermal link should ideally possess a high thermal conductivity to minimize temperature gradients or thermal lag between the crystal and the load.

When crossed by the laser beams, the crystal is re-emitting isotropically the absorbed laser power in the form of fluorescence, acting as an intense lightbulb. The link should possess a geometry minimizing the absorbed fluorescence power at the end of the link, while being the shortest possible

Table 5

CLOE characteristics

Dimensions (mm)	100 × 50 × 60
Volume (L)	0.3
Weight (kg)	1.0

to avoid thermal losses coming from the enclosure thermal radiation. There is an optical isolation between the thermal link and the focal plane to avoid radiation leakage.

The cooling head is attached to the cryostat containing the detector. In the case of a laser cooler, an aluminum cryostat measuring 160 mm × 180 mm and weighting 3.6 kg is considered. The CLOE sub-system is expected to fit in a volume of 0.3 L and weight 1 kg (Table 5). The CLOE along with the focal plane cryostat are shown in Figure 2.

3.2. Laser Electronics Assembly

The Laser Electronics Assembly (LEA) sub-system role is to:

- Convert the electrical power in optical power to feed the CLOE sub-system.
- Condition and acquire the temperature data measured in the CLOE sub-system.
- Regulate the cryogenic temperature at a reference point.
- Perform health checkups and report the results.

This subsystem is composed of a control and command module, a power generation module and an interface module. The LEA's main element is the laser diodes stage, converting the electrical power into optical power. The advantage of using laser diodes is that they can be stacked to reach the required power and they can be easily doubled.

The power stage assumes both the low power subsystem supply and the laser diodes current supply. A current amplifier allows the conversion of the command signal to power up the laser diodes. The LEA only comports DC power supplies so there is limited signal filtering.

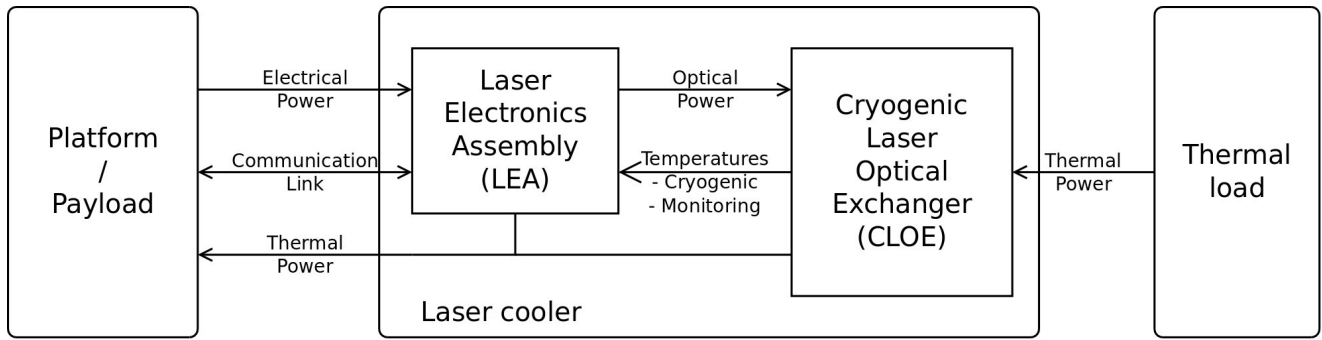


Figure 3: General architecture of a laser cooler. The cooling sub-system CLOE is located near the thermal load, whereas the control and power supply sub-system LEA can be located at any distance

Table 6
LEA characteristics

Dimensions (mm)	255 × 138 × 85
Volume (L)	3.0
Weight (kg)	2.0

The control and command module contains all the necessary elements to secure the laser diodes nominal operation: input current, photo-diode current, enclosure temperature monitoring. It performs a temperature regulation at the cooling point by the means of temperature acquisition and laser diode current feedback on that temperature.

The interface module assumes the outside link to the satellite platform. It gathers the modes management, protection and system surveillance information. The LEA characteristics are reported in Table 6.

4. Budget for a laser cooler architecture

4.1. Redundancy

The assumption of a high reliability satellite mission was made, requiring some form of redundancy for the cryocooler. Three options are possible: redundancy of the whole system, redundancy of only the electronics, or only the cold head. Although no reliability study for a laser cooler has been made so far, the assumption was made that the Laser Electronics Assembly has the highest failure probability due to the presence of power generation electronics and laser diodes. In the opposite, the cold head was assumed less likely to fail, with no known degradation of the optical cavity or the cooling crystal over time. Hence it was assumed in this study that only the electronics are redundant for a laser cooler, as shown in Figure 4.

4.2. Volume and weight

The total volume of a redundant laser cooler with cryostat is estimated approximately to 10 L. Accounting for 0.5 kg of cables, the total mass of the system and cryostat is estimated to 8.2 kg as shown in Table 7.

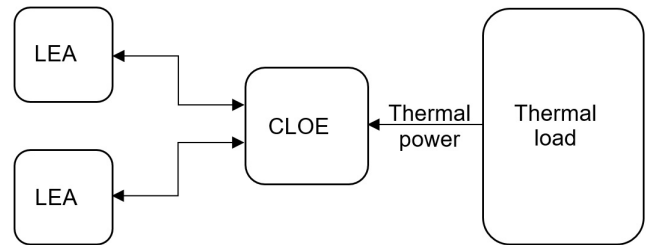


Figure 4: Diagram of the considered redundant LC architecture

Table 7
Volume and mass of a LC system

Equipment	Volume (L)	Mass (kg)
CLOE	0.3	1.0
2 × LEA	6.0	4.0
Cables	Negligible	0.5
Cryostat	3.6	2.7
Total	9.9 L	8.2 kg

4.3. Power consumption

4.3.1. Optical cooling efficiency

The cooling efficiency of a laser cooler is defined as the ratio of the generated heat lift over the laser power absorbed by the crystal. For state-of-the-art 10% doped Yb:YLF cooling crystals, it is estimated to 0.8 % at 120 K and 1.2 % at 150 K [27].

4.3.2. Thermal losses

From [9], thermal link losses for a laser cooler are the sum of two contributions :

- Heating due to the absorbed fluorescence at the end of the thermal link, P_{fluor}
- Heating due to the thermal radiation of the hot enclosure surrounding the cold crystal and thermal link assembly, P_{rad} .

The first contribution depends on the thermal link's geometry and its capability to reject the light coming from the

Table 8
 LC efficiency and thermal losses

	120 K	150 K
CLOE cooling efficiency (%)	0.8	1.2
Thermal link losses (mW)	30	30
Focal plane dissipation (mW)	280	280
Required cooling power (mW)	310	310
Required optical power (W)	38.8 W	25.8 W

Table 9
 LEA estimated efficiency

Command/control consumption	4 W
Power supply conversion efficiency	75 %
Laser diode optical conversion efficiency	55 %
Optical fiber coupling efficiency	90 %

Table 10
 Power requirements for a LC architecture

	120 K	150 K
CLOE input optical power (W)	38	26
Optical fiber losses (W)	4	3
LEA output optical power (W)	42	29
Conversion efficiency losses (W)	60	42
C/C consumption (W)	4	4
Total electrical power (W)	107 W	73 W

crystal. It is estimated to 22 mW at 135 K in a kinked thermal link with an inside angle of 15 °[9]. Assuming constant absorbed laser power between 120 K and 150 K (which is the case for $N > 50$ laser roundtrips inside the crystal [6]), the emitted fluorescence power P_{fluor} is the same at 120 K, 135 K and 150 K.

The second contribution depends on the surface of the crystal and thermal link which are in direct view of the enclosure's hot surface. It is estimated to 8 mW at 135 K for a $10 \times 4 \times 4$ mm crystal attached with the kinked thermal link previously cited [9]. To give an estimation at 120 K and 150 K, Stefan-Boltzmann law is applied :

$$P_{rad} \propto k(T_1^4 - T_2^4) \quad (6)$$

Taking $T_1 = 300$ K and $T_2 = 135$ K, the constant $k = 1.03 \times 10^{-12}$ is calculated. Replacing T_2 by its value yields $P_{rad} = 8.1$ mW at 120 K, and $P_{rad} = 7.8$ mW at 150 K. In the next part of the study, constant thermal link losses of 30 mW are considered at both 120 and 150 K.

4.3.3. Power conversion

The optical power P_{Opt} that has to enter the cavity is calculated from the required cooling power P_{Cool} and the optical cooling efficiency η_c :

$$P_{Opt} = \frac{P_{Cool}}{\eta_c} \quad (7)$$

Table 11
 Solar array sizing for a LC architecture

	120 K	150 K
Array power (W)	169	115
Array surface (m ²)	0.7	0.5
Array volume (L)	17.5	12.5
Array mass (kg)	1.8	1.3

Table 12
 Batteries sizing for a LC architecture

	120 K	150 K
Required capacity (Ah)	8.7	5.9
Number of cells	32 (8s4p)	24 (8s3p)
Dimensions (mm)	308 × 180 × 90	308 × 135 × 90
Volume (L)	4.9	3.7
Mass (kg)	4.9	3.7

Table 13
 Thermal control sizing for a LC architecture

Equipment	120 K	150 K	
Heat pipes	Dimensions	1.4 m, $\phi 11$ mm	1.4 m, $\phi 11$ mm
	Volume (L)	0.14	0.14
	Mass (kg)	0.47	0.47
Radiators	Surface (m ²)	0.25	0.17
	Volume (L)	0.38	0.26
	Mass (kg)	2.0	1.4
Total	Volume (L)	0.52	0.40
	Mass (kg)	2.5	1.9

The laser source power has to be superior by a factor k to account for fiber coupling losses, estimated at 10 %:

$$P_{Laser} = (1 + k)P_{Opt} \quad (8)$$

The required electrical power P_{Elec} is calculated from the electronics conversion efficiency:

$$P_{Elec} = \frac{P_{Laser}}{(\eta_{Laser}\eta_{PC})} + P_{LP} \quad (9)$$

with η_{Laser} the optical conversion efficiency, η_{PC} the electrical conversion efficiency from the PCDU to the LEA and P_{LP} the electronics low power part corresponding to the systems modes and acquisition.

Laser diodes and fiber amplifiers do exist in the near infrared at wavelengths, linewidth and powers that are suitable for cooling of rare-earth doped crystals. The efficiency of laser diodes in the near infrared is estimated to 50~60% [28]. For fiber lasers, the wall plug efficiency depends on both the pumping diodes efficiency and the fiber amplifier efficiency (50~80%), yielding a total efficiency of 25~50% [29]. A space qualified laser for cooling would only require adaptation and tests from an existing laser source.

Table 14
Satellite SWaP summary for a LC architecture

Equipment	120 K			150 K		
	Volume (L)	Mass (kg)	Power (W)	Volume (L)	Mass (kg)	Power (W)
Payload						
CLOE	0.3	1.0		0.3	1.0	
2 × LEA	6	4.0		6	4.0	
Cables	Negligible	0.5		Negligible	0.5	
Cryostat	3.6	2.7		3.6	2.7	
Payload total	9.9	8.2	107	9.9	8.2	73
Platform						
Solar array	17.5	1.8		7.5	0.8	
Batteries	4.9	4.9		3.7	3.7	
Thermal control	0.5	2.5		0.4	1.9	
Platform total	22.9	9.2		11.6	6.4	
Total without margin	32.8	17.4	107	21.5	14.6	73
Structure margin (+25 % mass)		4.4			3.7	
Total with margin	32.8 L	21.8 kg	107 W	21.5 L	18.3 kg	73 W

In this study, a laser diode with an optical conversion efficiency η_{Laser} of about 55 % is assumed. The electrical conversion efficiency η_{PC} is estimated to 75 %. The low power part P_{LP} is based on the Cryocooler Drive Electronics of a MPTC, applying a power reduction due to a simplified control and command module. It is estimated to 4 W.

The power sizing of a laser cooler is summarized in Table 10. To reach 120 K, 38 W of optical power need to be supplied to the cavity, resulting in 106 W of electrical consumption for the whole system. At 150 K, an optical power of 26 W is needed, resulting in 75 W of consumption.

4.4. Solar array and batteries sizing

Knowing the required power for a laser cooler, the solar array and batteries sizing for both temperatures is performed. To calculate the solar array surface it is necessary to take into account the continuous cryocooler operation plus an additional consumption due to the batteries charging during daytime. We have the following relationship:

$$P_{SA} = \frac{1}{T_S} \left(\frac{PT_S}{\epsilon_{DET}} + \frac{PT_E}{\epsilon_C} \right) \quad (10)$$

With P_{SA} the required solar array power, P the payload power, T_S the orbit sun-time and T_E the orbit eclipse time, ϵ_{DET} the solar array to payload direct energy transfer efficiency, ϵ_C the batteries charging efficiency. Taking $\epsilon_{DET} = 98\%$ [15] and $\epsilon_C = 95\%$ we have:

$$P_{SA} = P \left(\frac{65.3 + 35.8}{64} \right) \quad (11)$$

The batteries are sized to support the continuous cryocooler operation over a 34 minutes eclipse (0.57 h). The required capacity (in Wh) is calculated knowing the system

power consumption, with 30 % DOD, a capacity fading $\eta_B=88\%$ and a discharge efficiency $\epsilon_D = 95\%$. We have:

$$C_B = \frac{PT_E}{DOD\eta_B\eta_D} = \frac{P \times 0.57}{0.30 \times 0.88 \times 0.95} = P \times 2.27 \quad (12)$$

The cells are mounted in series to reach the required bus voltage, and then in parallel to reach the required capacity. For 3.6 V cells, 8 cells in series are needed to reach 28 V. The number of parallel cells is calculated from the required capacity (in Ah) divided by the capacity of one cell and multiplied by two for redundancy:

$$p = \frac{C_B}{C_{Cell}} \times 2 \quad (13)$$

Finally, the number of required cells is found. Batteries size, volume and mass are calculated proportionally from Saft VES16 8s4p battery, measuring $308 \times 180 \times 90 \text{ mm}^3$ and weighting 4.9 kg [19]. Batteries sizing for a laser cooler architecture is summarized in Table 12.

4.5. Thermal control sizing

The heat dissipated by fluorescence amounts to 38 W at 120 K and 26 W at 150K. To regulate the system, 11 mm diameter aluminum-ammonia heatpipes are used, capable to extract a maximal heat of 50 W m [22]. Assuming a 1 m side satellite, a heat pipe needs to cover about 0.5 m from the center to the nearest satellite face. Heat pipes have to be tethered to a radiator and thus a higher heat pipe length is needed. Two heat pipes of 0.7 m each are assumed. With a linear mass of 0.34 kg/m for $\phi 11$ mm aluminum heatpipes [22], a mass of 0.47 kg is found. The radiators surfaces, masses and volumes are calculated using the values given in subsection 2.6. Thermal control sizing is summarized in Table 13.

Table 15
CMA characteristics

Dimensions (mm)	250 × 150 × 140
Volume (L)	5.5
Weight (kg)	3.9

Table 16
CDE characteristics

Dimensions (mm)	255 × 138 × 55
Volume (L)	1.9
Weight (kg)	1.4

4.6. Laser cooler at satellite level: summary

Adding the volumes and masses previously calculated the payload, platform and satellite level total volumes and masses are found for a laser cooler architecture (Table 14). As expected with a miniaturized cooling head, the payload impact in terms of mass and volume is modest, while at satellite level most of the volume is contained in the solar array and batteries.

5. Miniature Pulse Tube Cooler architecture

To this day, pulse tube coolers are the standard cryocoolers used in the range 10 K to 200 K [30]. A Miniature Pulse Tube Cooler is composed of a Cryocooler Mechanical Assembly (CMA) powered by a Cryocooler Drive Electronic (CDE).

5.1. Cryocooler Mechanical Assembly

The Cryocooler Mechanical Assembly sub-system is composed of a compressor generating an oscillating high pressure wave, going through a pulse tube. A "cold finger" is attached between the cold end of the pulse tube and the focal plane. The whole sub-system is supported by mechanical dampeners and accelerometers in order to monitor and decrease vibrations levels. The CMA role is to:

- Supply electrical power to the compressor at the pulse tube input with a waveform piloted by the CDE in order to convert mechanical power into heat lift.
- Measure the cold finger temperature and the micro-vibrations levels and report them to the CDE.

From previous miniature pulse tube coolers prototypes developed at Air Liquide Advanced Technologies for 80 K - 200 K range observation missions [31, 32], a MPTC-CMA occupies a volume of 5.5 L and weight 3.9 kg (Table 15).

5.2. Cryocooler Drive Electronics

The Cryocooler Drive Electronics role is to:

- Acquire the temperature and forces reported by the CMA.
- Pilot with precision the cold finger temperature.

Table 17
Volume and mass of a MPTC system

Equipment	Volume (L)	Mass (kg)
2 × CMA	11.0	7.8
2 × CDE	2.8	2.8
Cables	Negligible	1.0
Cryostat	9.4	5.4
Total	23.2 L	17.0 kg

Table 18
CMA efficiency, losses and required cooling power

	120 K	150 K
CMA cooling efficiency (%)	9	12
Cold redundancy losses (mW)	320	320
Focal plane dissipation (mW)	280	280
Required cooling power (mW)	600	600
Required electrical power (W)	7	5

- Reduce electronically through a feedback loop the micro-vibrations in the CMA.

Just like the LEA sub-system in the laser cooler architecture, a CDE is composed of a control and command module, a power generation module and an interface module. The CDE characteristics are reported in Table 16.

5.3. Volume and weight

For the Miniature Pulse Tube Cooler architecture, a cold redundancy with two CMA and two CDE is assumed: one cooler is active while the other one is off. The cryostat has to be bigger than in the laser cooler setup to be able to fit two cold fingers and a thermal braid linked to the focal plane. In the case of a MPTC, the aluminum cryostat measures 200 mm × 300 mm and weights 5.4 kg. The redundant CMA along with the focal plane cryostat are shown in Figure 5. The total volume is estimated to 23 L as summarized in Table 17. For the mass estimation, the following items were taken into account:

- The masses of two CMA and two CDE
- The expected cryostat mass
- The cables mass between the CMAs and CDEs

The total mass is estimated to 18 kg as summarized in Table 17.

5.4. Power consumption

5.4.1. Cooling efficiency

The cooling efficiency of a pulse tube is defined as the ratio of the generated heat lift over the compressor electrical power. It is estimated to 9 % (11.1 W/W) at 120 K, and 12 % (8.3 W/W) at 150 K for a MPTC.

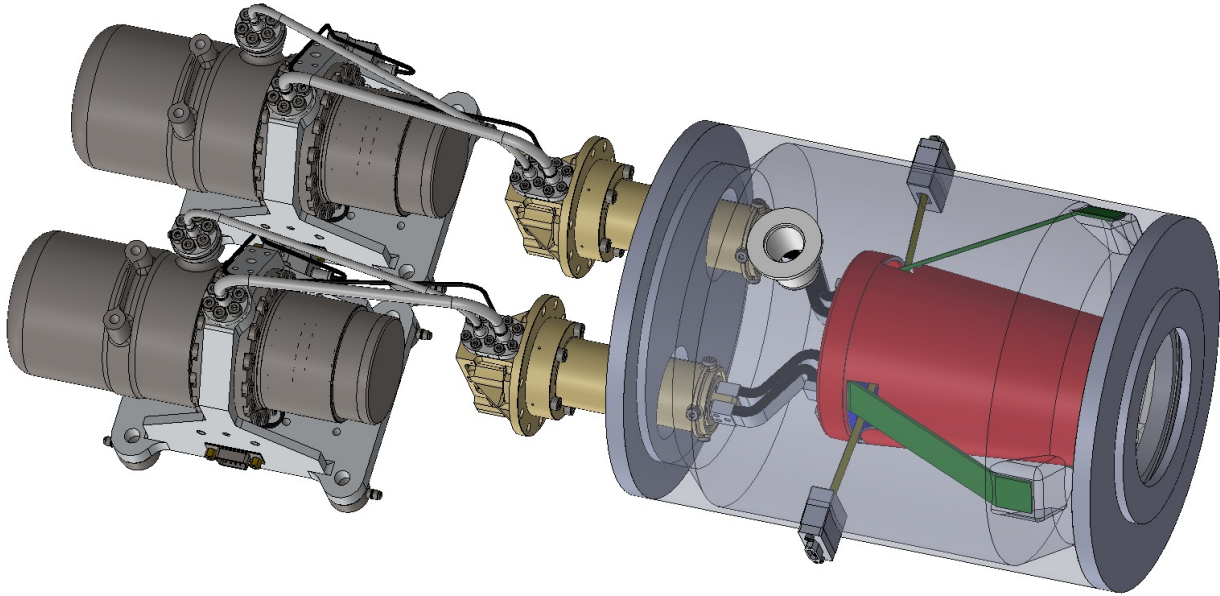


Figure 5: Concept of a focal plane architecture with redundant Miniature Pulse Tube Coolers. The electronics are not shown. The scale is the same as Figure 2.

Table 19
Power requirements for a MPTC architecture

	120 K	150 K
CMA electrical power (W)	7	5
CDE electrical power (W)	7	7
Total electrical power (W)	14	12

Table 20
Solar array sizing for a MPTC architecture

	120 K	150 K
Array power (W)	22	19
Array surface (m ²)	0.09	0.08
Array volume (L)	2.3	2.0
Array mass (kg)	0.23	0.20

Table 21
Batteries sizing for a MPTC architecture

	120 K	150 K
Required capacity (Ah)	1.1	1.0
Number of cells	8 (8s1p)	8 (8s1p)
Dimensions (mm)	308 × 45 × 90	308 × 45 × 90
Volume (L)	1.3	1.3
Mass (kg)	1.3	1.3

5.4.2. Thermal losses

Cold redundancy implies that a part of the cooling power from the working CMA is wasted in parasitic losses when cooling the second and warmer cold finger. Those cold redundancy losses are estimated to 320 mW. To extract 280 mW off the focal plane, a CMA cooling power of 600 mW

Table 22
Thermal control sizing for a MPTC architecture

Equipment		120 K	150 K
Heat pipes	Size	2.8 m, ø11 mm	2.8 m, ø11 mm
	Volume	0.27 L	0.27 L
	Mass	0.94 kg	0.94 kg
Radiators	Size	0.09 m ²	0.08 m ²
	Volume	0.14 L	0.12 L
	Mass	0.36 kg	0.32 kg
Total	Volume	0.41 L	0.39 L
	Mass	1.3 kg	1.3 kg

is required. The CMA cooling efficiency, losses and power requirements are summarized in Table 18.

5.4.3. Power conversion

The CMA consumption is calculated from the cooling efficiency: a CMA consumption of 7 W is estimated for 120 K and 5 W for 150 K. The CDE consumption variation is assumed marginal and estimated to a constant 7 W (Table 19).

5.5. Solar array and batteries sizing

Knowing the consumption of a MPTC, the required solar array power, surface, volume and mass are calculated and summarized in Table 20. Based on the same assumptions as before, the batteries requires a capacity of 1 Ah at both 120 and 150 K. Due to the need of a 28 V output, the minimal battery is a 8s1p with a total capacity of 4.5 Ah which is more than twice the required capacity, taking redundancy into account. 1.3 kg of batteries are found for a MPTC. That mass would be lower in a real satellite, due to the presence of other equipment and the possibility to adjust the number

Table 23
Satellite SWaP summary for a MPTC architecture

Equipment	120 K			150 K		
	Volume (L)	Mass (kg)	Power (W)	Volume (L)	Mass (kg)	
Payload						
2 × CMA	11	7.8		11	7.8	
2 × CDE	2.8	2.8		2.8	2.8	
Cables	Negligible	1.0		Negligible	1.0	
Cryostat	9.4	5.4		9.4	5.4	
Payload total	23.2	17.0	14	23.2	17.0	12
Platform						
Solar array	2.3	0.2		2.0	0.2	
Batteries	1.3	1.3		1.3	1.3	
Heat pipes	0.3	0.9		0.3	0.9	
Radiators	0.1	0.4		0.1	0.3	
Platform total	4.0	2.8		3.7	2.7	
Total without margin	27.2	19.8	14	26.9	19.7	12
Structure margin (+25 % mass)		5.0			4.9	
Total with margin	27.2 L	24.8 kg	14 W	26.9 L	24.6 kg	12 W

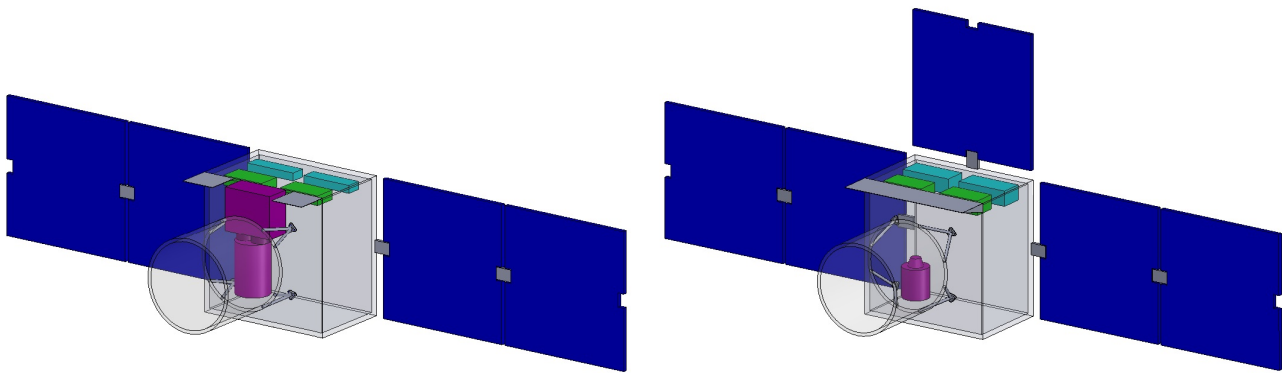


Figure 6: Visual comparison between Miniature Pulse Tube Cooler (left) and Laser Cooler (right) architectures onboard an observation microsatellite at 150 K. Cryocooler and cryostat are shown in purple, electronics in green, batteries in cyan.

of parallel cells for higher capacities. However for this study the analysis is based on a standalone system. Batteries sizing for a pulse tube architecture is summarized in Table 21.

5.6. Thermal control sizing

To evacuate the heat off the warm side of the two CDE, 4 pipes of 11 mm diameter were chosen, with the previous hypotheses for heat pipes and radiator masses. Thermal control sizing is summarized in Table 22.

5.7. MPTC at satellite level: summary

Volume, mass and power requirements for a Miniature Pulse Tube Cooler architecture at satellite level are summarized in Table 23. For almost 300 mW cooling at 120-150 K, cold redundancy implies a required cooling power twice as high due to thermal losses. Although the power consumption stays low at those temperatures, two-thirds of the mass and 85% of the volume are contained in the satellite payload.

6. Discussion

Our main results comes from the comparison of Table 14 and Table 23, as summarized in Table 24. The satellite analysis shows that despite a higher total volume is needed mainly due to the increased solar array surface, the LC architecture is expected to weight less than a MPTC architecture and occupies less internal volume for both 120 K and 150 K. Figure 6 features a visual comparison between the two architectures on-board a micro-satellite.

7. Conclusions

This study shows that laser cooling is a promising technology for the miniaturization of observation satellites. Using the same mission scenario, it is found that a laser cooler is favorable in terms of mass and internal volume savings compared to a Miniature Pulse Tube Cooler. Additionally, this solution presents other great advantages over mechani-

Table 24
SWaP analysis summary

	Laser Cooler		Miniature Pulse Tube Cooler	
	120 K	150 K	120 K	150 K
Power consumption	107 W	73 W	14 W	12 W
Satellite volume (Internal volume)	32.8 L (15.3 L)	21.5 L (14 L)	27.2 L (24.9 L)	26.9 L (24.9 L)
Satellite mass	21.8 kg	18.3 kg	24.8 kg	24.6 kg

cal cryocoolers:

- Zero vibrations generated due to the absence of moving parts.
- No electromagnetic perturbations near the focal plane.
- A smaller cryostat, less cables and simplified operation compared to a mechanical cryocooler.
- A simpler redundant architecture. Assuming that the cold head is less likely to fail being constituted of passive optical elements, only the electronics redundancy was considered, implying no thermal losses due to the cold head doubling.
- Increased payload flexibility with a compact cryocooler expected to fit in the volume of a glass of water.
- Increased platform flexibility with the cryocooler's power being supplied through an optical fiber, allowing the laser electronics to be located anywhere in the satellite.

All these advantages make possible the accommodation of a laser cryocooler on-board future low earth orbit small satellites as an innovative and breakthrough vibration-less alternative to mechanical cryocoolers in the 100 K - 200 K range, keeping in mind that laser cooling in solids is still a low TRL technology and has a wide potential for improvement in terms of cooling efficiency [33].

8. Acknowledgments

Rémi Vicente thanks the french National Association for Research and Technology (ANRT), Air Liquide Advanced Technologies and Institut Néel for his PhD funding under CIFRE contract number 2018-0065. This work was conducted following a pre-study made by Arnaud Gardelein, Jean-Michel Niot and Pierre Contini, funded thanks to Air Liquide Advanced Technology innovation comity.

References

- [1] R. I. Epstein, M. I. Buchwald, B. C. Edwards, T. R. Gosnell, C. E. Mungan, Observation of laser-induced fluorescent cooling of a solid, *Nature* 377 (1995) 500.
- [2] B. C. Edwards, M. I. Buchwald, R. I. Epstein, T. R. Gosnell, C. E. Mungan, Development of a Fluorescent Cryocooler, 9th American Institute of Astronautics & Aeronautics Conference on Small Satellites (1995).
- [3] G. L. Mills, A. J. Mord, P. A. Slaymaker, Design and Predicted Performance of an Optical Cryocooler for a Focal Plane Application, *Cryocoolers* 11 (2002) 613–620.
- [4] E. Pettyjohn, Cryocoolers for Microsatellite Military Applications, *Cryocoolers* (2008) 6.
- [5] S. Melgaard, D. Seletskiy, V. Polyak, Y. Asmerom, M. Sheik-Bahae, Identification of parasitic losses in Yb:YLF and prospects for optical refrigeration down to 80 K, *Optics Express* 22 (2014) 7756.
- [6] A. Gragossian, J. Meng, M. Ghasemkhani, A. R. Albrecht, M. Sheik-Bahae, Astigmatic Herriott cell for optical refrigeration, *Optical Engineering* 56 (2016) 011110.
- [7] J. Parker, D. Mar, S. Von der Porten, J. Hankinson, K. Byram, C. Lee, M. K. Mayeda, R. Haskell, Q. Yang, S. Greenfield, R. Epstein, Thermal links for the implementation of an optical refrigerator, *Journal of Applied Physics* 105 (2009).
- [8] A. Gragossian, M. Ghasemkhani, J. Meng, A. Albrecht, M. Tonelli, M. Sheik-Bahae, Optical refrigeration inches toward liquid-nitrogen temperatures, *SPIE Newsroom* (2017).
- [9] M. P. Hehlen, J. Meng, A. R. Albrecht, E. R. Lee, A. Gragossian, S. P. Love, C. E. Hamilton, R. I. Epstein, M. Sheik-Bahae, First demonstration of an all-solid-state optical cryocooler, *Light: Science & Applications* 7 (2018) 15.
- [10] G. Cittadino, A. Volpi, A. Di Lieto, M. Tonelli, Czochralski crystal growth for laser cooling, *Optical Engineering* 56 (2017).
- [11] F. Buisson, An updated status of MicroCarb Project, *IWGGMS-14* (2016).
- [12] R. J. Boain, ABCs of Sun-Synchronous Orbit Mission Design, 14th AAS/AIAA Space Flight Mechanics Meeting (2004) 20.
- [13] B. Nadir, MIT Open Courses, Satellite Engineering, 2003. URL: <https://ocw.mit.edu/courses/aeronautics-and-astronautics/16-851-satellite-engineering-fall-2003/>.
- [14] A. Delannoy, B. Fièrque, P. Chorier, C. Riuné, Ngp: a new large format infrared detector for observation, hyperspectral and spectroscopic space missions in visir, swir and mwir wavebands, *Proc. of SPIE* 9639 (2013).
- [15] E. Lapeña, J. L. Herranz, F. Gómez-Carpintero, M. Rodríguez, The LEO PCDU EVO - A Modular and Flexible Concept for Low to Medium Power LEO & Scientific Missions, *E3S Web of Conferences* 16 (2017) 18009.
- [16] W. Guter, L. Ebel, D. Fuhrmann, W. Köstler, M. Meusel, Development, qualification and production of space solar cells with 30 % EOL efficiency, 10th European Space Power Conference Proceedings (2014).
- [17] SpaceTech GmbH, Solar arrays product information, 2019. URL: <https://spacetechnology.com/products/subsystems/solar-arrays/>.
- [18] M. Imaizumi, T. Takamoto, N. Kaneko, Y. Nozaki, T. Ohshima, Qualification Test Results of IMM Triple-Junction Solar Cells, Space Solar Sheets, and Lightweight&Compact Solar Paddle, *E3S Web of Conferences* 16 (2017) 03012.
- [19] D. Y. Borthomieu, S. Remy, VES16 cells and batteries for LEO & small GEO, 11th European Space Power Conference Proceedings (2014).
- [20] S. Remy, D. Prevot, D. Reulier, D. F. Vigier, VES16 Li-Ion Cell For Satellite, 9th European Space Power Conference Proceedings (2011).
- [21] D. Prevot, Y. Borthomieu, E. Ligneel, R. Hague, J.-P. Peres, C. Cenac-Morthe, Performances of Saft Lithium-Ion Cells in LEO Cycling,

- E3S Web of Conferences 16 (2017) 06005.
- [22] C. Hoa, B. Demolder, A. Alexandre, Roadmap for developing heat pipes for ALCATEL SPACE's satellites, *Applied thermal engineering* 23 (2003).
 - [23] J. Schilke, A. Natusch, H. Ritter, BepiColombo Radiator Breadboard Performance Test, *Proceedings of the 38th International Conference on Environmental Systems* (2008).
 - [24] J. H. Saleh, D. E. Hastings, D. J. Newman, Spacecraft design lifetime, *Journal of Spacecraft and Rockets* 39 (2002).
 - [25] Almecogroup, TiNOX energy, 2019. URL: <https://www.almecogroup.com/en/pagina/53-tinox-energy-cu>.
 - [26] Acktar, Acktar Nano Black, 2019. URL: <https://www.acktar.com/product/nano-black/>.
 - [27] S. D. Melgaard, A. R. Albrecht, M. P. Hehlen, M. Sheik-Bahae, Solid-state optical refrigeration to sub-100 Kelvin regime, *Scientific Reports* 6 (2016) 20380.
 - [28] Jenoptik, Jenoptik laser diodes array DL-BAB-50-23-1020-TE-120-2.0, 2019. URL: <https://www.jenoptik.com/products/lasers/high-power-diode-lasers/selector/semiconductor-material-high-power-diode-lasers?variantId=819b73a3-1fd9-4812-9007-1563b928d8fc>.
 - [29] C. Ottenhues, T. Theeg, K. Hausmann, M. Wyszomolek, H. Sayinc, J. Neumann, D. Kracht, Single-mode monolithic fiber laser with 200 W output power at a wavelength of 1018 nm, *Optics Letters* 40 (2015).
 - [30] Air Liquide Advanced Technologies, Active cryo cooling for space application, turnkey solutions from 10K to 200K, 2019. URL: <https://advancedtech.airliquide.com/pulse-tubes>.
 - [31] T. Trollier, J. Tanchon, J. Buquet, A. Ravex, Status of Air Liquide space pulse tube cryocoolers, *Cryocoolers* 15 (2009).
 - [32] C. Chassaing, J. Butterworth, G. Aigouy, C. Daniel, M. Crespin, E. Duvivier, 150K – 200K Miniature Pulse Tube Cooler for Micro Satellites, *Advances in Cryogenic Engineering, AIP Conference Proceedings* 1573 (2014).
 - [33] S. Rostami, A. Volpi, A. R. Albrecht, M. Sheik-Bahae, Progress towards optical cryocooling in Mid-IR, *Photonic Heat Engines: Science and Applications, Proceedings of SPIE* 10936 (2019).